Nitrogen-Induced Catalyst Restructuring for Epitaxial Growth of Multiwalled Carbon Nanotubes

Sebastian W. Pattinson, Vinay Ranganathan, Hajime K. Murakami, Krzysztof K. K. Koziol,* and Alan H. Windle*

Department of Materials Science and Metallurgy, University of Cambridge, Pembroke Street, Cambridge CB2 3QZ, United Kingdom

ABSTRACT

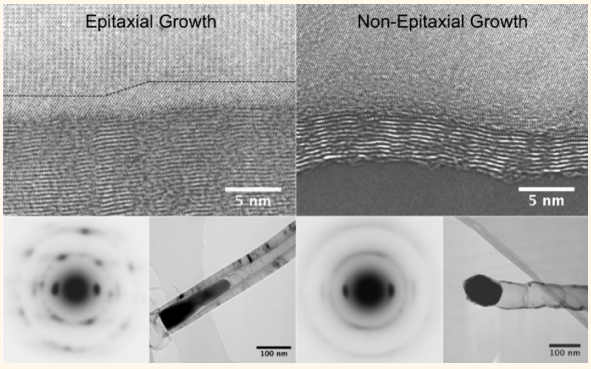

The ability to simply and economically produce carbon nanotubes (CNTs) with a defined chiral angle is crucial for the exploitation of nanotubes for their electrical properties. We investigate a diverse range of nitrogen sources for their ability to control CNT chiral angle *via* epitaxial growth from highly ordered catalyst particles. Through the use of *in situ* mass and infrared spectrometry, we elucidate the mechanism by which these ordered catalyst particles are formed, showing that ammonia is a key intermediate in the process. Subsequently, the direct addition of a small amount of ammonia to an otherwise standard CNT synthesis is shown to be able to form catalyst particles that grow single chiral angle multiwalled carbon nanotubes. Variation in the ammonia concentration clarifies the catalyst restructuring necessary for the epitaxial growth of carbon nanotubes and subsequent chiral angle control. The simple addition of a nitrogen source is an attractive route for chiral angle control; however, the model also suggests further ways to optimize CNT chiral angle distributions as well as to improve CNT and graphene yield and crystallinity. This understanding also explains the action of ammonia in its widely used role in activating catalyst prior to CNT growth. Finally, this work highlights the uses of novel surface geometries that are achievable through multiphase catalysts.

KEYWORDS: catalyst restructuring · epitaxial growth · multiwalled carbon nanotubes · chemical vapor deposition · chirality control · nitrogen carbon nanotubes

The control of the chiral angle, and thereby electrical properties, of carbon nanotubes remains the single most pressing barrier to the use of CNTs in many applications. This is because approximately one-third of nanotubes feature metallic properties, while the remainder behave as semiconductors, limiting their usefulness.[1] Many different approaches to address this have been developed. These can be divided into methods that sort the nanotubes after synthesis and those which seek to produce only nanotubes with a particular electrical type or chiral angle. Sorting methods have made significant progress using a variety of techniques including wrapping by single-stranded DNA and then separation by anion exchange chromatography;[2] selective etching by a plasma hydrocarbon reaction;[3] attachment of surfactants and subsequent density gradient ultracentrifugation;[1] precipitation following chemical treatment;[4] adsorption of CNTs on agarose and freezing followed by mechanical separation;[5] and *in situ* and postsynthesis oxidation.[6] DNA sorting techniques have even recently separated CNTs by chiral angle.[7] Often, however, the processing steps involved in these techniques are difficult, reduce yield, and are unsuitable for applications requiring significant quantities of CNTs.

Such difficulties partly motivate efforts to directly grow CNTs with a particular chiral angle distribution. These are also striking in their diversity and include varying the noble gas and oxidative and reductive species present during thermal annealing of catalyst;[8] the application of UV radiation during synthesis;[9] the addition of methanol to synthesis on single crystal quartz substrates;[10] the use of bimetallic growth catalyst at low reaction temperature;[11] using nonmagnetic catalyst in plasma-enhanced chemical vapor deposition (CVD);[12] and the use of rapid heating in plasma-enhanced CVD.[13] In addition to the above techniques, which mostly involve single-walled CNTs, multiwalled CNTs with identical chiral angle in each layer have also been produced by low-temperature plasma-enhanced CVD[14] and pyrolysis of iron phthalocyanine.[15] The possible chiral angles of such multiwalled CNTs are constrained because the graphene

* Address correspondence to ahw1@cam.ac.uk, kk292@cam.ac.uk.

Received for review April 5, 2012 and accepted August 1, 2012.

Published online August 01, 2012
10.1021/nn301517g

interlayer spacing must be maintained while also allowing the graphene sheet to close itself as a cylinder.[16] Despite intensive research, the mechanisms by which the chiral angle is influenced are often only partially understood, feature low yields, or otherwise require very specific conditions that would be difficult to reproduce industrially.

Ammonia has been used extensively in CNT synthesis, primarily as a means of "activating" the catalyst prior to CNT growth,[17−19] as well as in carbon nanofiber synthesis.[20] Recently, it has also been suggested that ammonia is able to influence chiral angle distribution in single-walled CNTs,[21] though the mechanism for this is unclear and, therefore, it is difficult to formulate strategies toward producing useful (fully metallic or fully semiconducting) chiral angle distributions with it.

We have shown that the addition of pyrazine to the feedstock for carbon nanotube synthesis can produce dense arrays of perfectly straight multiwalled carbon nanotubes.[22] Most importantly, these CNTs feature either armchair or zigzag chiral angles in every layer of their structure, suggesting that this method could be used to produce whole arrays of nanotubes with a controlled chiral angle. More recently, we have proposed a model to understand the growth of such CNTs based on epitaxy and belt nucleation from the highly ordered catalyst particles that produce these nanotubes.[23] Specifically, these catalyst particles are always Fe_3C, with the nanotube axis aligned with the [100] plane of the catalyst, and feature a restructured surface layer of iron, which is able to epitaxially grow CNT walls. The implication is that the epitaxy requires an oriented iron carbide catalyst, and that pyrazine is necessary for the formation of such a catalyst particle.

This report explores the relationship between the form of the added nitrogen and the observation of single chiral angle multiwalled nanotubes, showing that a very wide range of nitrogen sources can cause chiral angle control. To explain this generality, we used *in situ* techniques to look at the chemistry of the synthesis process and thus at the mechanism of catalyst restructuring. We found that ammonia is a key intermediate for producing highly ordered catalyst particles, and, on its own, is able to produce multiwalled carbon nanotubes in which each layer has a chiral angle corresponding to metallic electrical properties. We use high-resolution electron microscopy of the catalyst/nanotube interface to explain how ammonia is, when supplied at an appropriate level, able to induce catalyst restructuring leading to the formation of a surface layer from which nanotubes are able to epitaxially grow. We use this to explain why the effect is seen using many nitrogen sources and suggest strategies for applying this insight to producing arrays of single chiral angle carbon nanotubes on a larger scale and to improve carbon nanostructure synthesis more generally. Our findings also suggest a mechanism explaining why ammonia is effective in activating catalyst prior to CNT growth.

RESULTS AND DISCUSSION

Variation of Nitrogen Source. Building on our work with pyrazine,[22] we explored a wide variety of nitrogen-containing molecules, covering many different structures, to see which would be able to produce single chiral angle carbon nanotubes. As shown in Table 1, the additional molecules we selected were pyridine, triazine, nitrogen gas, benzylamine, aniline, and acetonitrile.

Of these molecules, pyridine, pyrazine, triazine, benzylamine, and acetonitrile were able to produce single chiral angle CNTs. These were primarily in either the armchair (chiral angle 30°) or zigzag configuration (chiral angle 0°), as evidenced in the electron diffraction patterns shown in Table 1, and as expected given that prior studies of CNTs grown with pyrazine showed that 20% were armchair, 30% zigzag, and the remainder a superposition of these two chiralities.[22] These highly crystalline single chiral angle CNTs were formed in well-aligned and dense arrays (Figure 1 SEM images), though the nanotubes grown using acetonitrile have noticeably lower numerical density per unit substrate area than the other nitrogen sources producing single chiral angle CNTs. Similarly, the single chiral angle CNTs all featured internal membranes, thin layers of graphene perpendicular to the axis of the CNT, as previously shown using pyrazine.[22] The arrays formed by these CNTs were also noticeably shorter than those produced without nitrogen, implying a lower growth rate. The nanotubes themselves, however, tended to have a large diameter due to the similarly large diameter of the catalyst, potentially a result of the prevention of catalyst loss into the CNT core by the internal membranes.[24] The nitrogen content of these CNTs was quite low, between 1 and 6 wt %, indicating that little of the nitrogen in the reactor was being incorporated into the CNTs, in some cases, such as 95 wt % benzylamine, significantly less than the C/N ratio in the feedstock. This is to be expected, though, given that much of the nitrogen is found as nitrogen gas in the hollow core of the CNTs.[16]

Nitrogen gas and 95 wt % aniline solution produced multichiral angle CNTs as did the sample with no nitrogen precursor. The array of CNTs grown in nitrogen gas appears identical to that grown with no nitrogen in an argon atmosphere. The TEM images of the 95 wt % aniline sample show that these nanotubes are both defective and feature internal membranes. Additionally, this sample contained many iron particles coated in carbon that were not able to grow CNTs at all. The feedstock containing 20 wt % aniline (in toluene) produced a mixture including significant proportions of both single and multichiral angle CNTs, all of which

TABLE 1. Results of Syntheses Using Different Nitrogen Sources, As Shown by SEM, TEM, Electron Diffraction from Individual Multiwalled Nanotubes and N Content[a]

Feedstock	SEM	TEM	Electron diffraction	N wt.%
95wt.% toluene	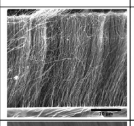	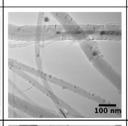		0.0
20wt.% pyridine 75wt.% toluene 	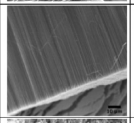	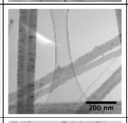	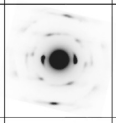	1.8
20wt.% pyrazine 75wt.% toluene 	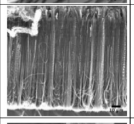	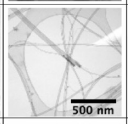	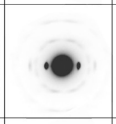	6.2
20wt.% triazine 75wt.% toluene 	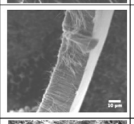	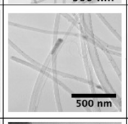	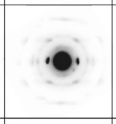	5.8
95wt.% toluene N_2 atmosphere $N\equiv N$	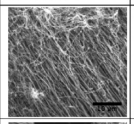	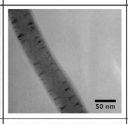		0.0
20wt.% benzylamine 75wt.% toluene 	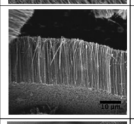	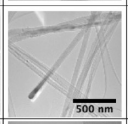	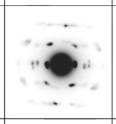	0.8
95wt.% benzylamine 	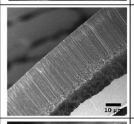	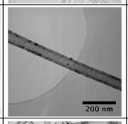	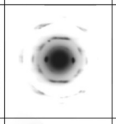	2.5
20wt.% aniline 75wt.% toluene 	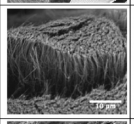	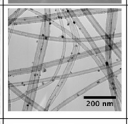	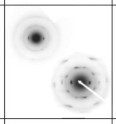	1.7
95wt.% aniline 	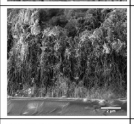	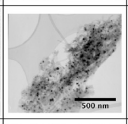	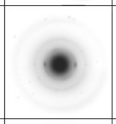	2.6
20wt.% acetonitrile 75wt.% toluene $CH_3—C\equiv N$	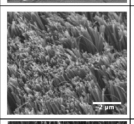	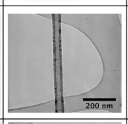	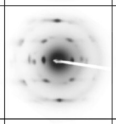	1.3
20wt.%toluene 75wt.% acetonitrile $CH_3—C\equiv N$	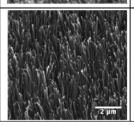	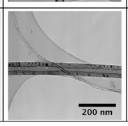	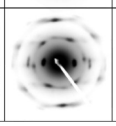	3.5

[a] All samples were grown with 5 wt % ferrocene in the feedstock as catalyst source. With the exception of aniline and nitrogen gas, all of the nitrogen sources produce well-ordered arrays of single chiral angle CNTs, as demonstrated by electron diffraction patterns featuring distinct reflections beyond just the 002 graphite planes seen in all multiwalled CNTs. The patterns shown indicate either armchair or zigzag CNTs; 20 wt % aniline in the feedstock (with toluene) produces a mixture of single and multichiral angle CNTs, while 95 wt % aniline produces poor-quality CNTs that have multiple chiral angles, as well as many carbon-coated iron particles.

had internal membranes. The nitrogen content of the sample grown in nitrogen gas and the non-nitrogen CNTs was zero, while in the aniline samples, it was between 1 and 3 wt %.

As can be seen in Table 1, a wide variety of nitrogen sources can produce single chiral angle CNTs, with aniline and nitrogen gas being the only sources investigated to produce predominantly multichiral angle CNTs. We decided to look more closely at benzylamine and aniline because these produced, respectively, high- and low-quality CNTs when mixed with just ferrocene. Using *in situ* mass spectrometry and FTIR, this would give us a clear picture of which species are present in the reactor without interfering signals created by toluene.

***In Situ* Characterization of Reaction.** We used mass spectrometry and FTIR with the probe inserted directly into the reaction zone to gain insight into the synthesis as it occurred. These results can be seen in Figure 1. Under reaction conditions, benzylamine completely decomposes to form benzene, toluene, and benzonitrile, which are the peaks at 78, 91, and 103 *m/z*, respectively, as well as ammonia, which is the peak at 17 *m/z*. The absence of a peak at 106 also shows that benzylamine has completely decomposed. This decomposition is well-documented and what would be expected from benzylamine even without catalyst at these temperatures.[25] The peak at 28 *m/z* is present even with no feedstock injected and is therefore most likely nitrogen gas contamination. The FTIR spectrum also supports this decomposition pathway. The peak at 3067 cm^{-1} corresponds to the aromatic C—H stretch; the peak at 1495 cm^{-1} is that of C═C stretching; and the peak at 677 cm^{-1} corresponds to the out-of-plane C—H bending mode, all of which are consistent with benzene. The peaks at 930 and 965 cm^{-1} show the symmetric bending mode of ammonia. These results show that nitrogen primarily takes the form of ammonia with benzylamine feedstock under reaction conditions, and that this is therefore also most likely the form in which it interacts with the catalyst.

The mass spectrum of CNT synthesis with aniline suggests that it does not significantly decompose in the reactor. The peaks at 46, 52, 78, and 93 *m/z* are attributable to aniline, while the remaining peaks result from the carrier gas. This is also in line with expectations from the literature given the stability of aniline.[26] The FTIR results also support this conclusion in that the peaks are consistent with aniline. The peak at 3038 cm^{-1} is the aromatic C—H stretching mode; the peak at 1611 cm^{-1} is the NH_2 bending mode; the peak at 1491 cm^{-1} is the C═C stretching mode; 1262 cm^{-1} is the C—N stretching mode, and the peaks at 742 and 668 cm^{-1} are the out-of-plane C—H bending mode.

From these measurements, it appears likely that nitrogen arrives at the catalyst in the form of aniline, which is relatively stable. This potentially also explains why there are so many deactivated catalyst particles in the sample produced in pure aniline: the iron catalyst is unable to crack the aniline that arrives at its surface, leading to the blockage of active sites.

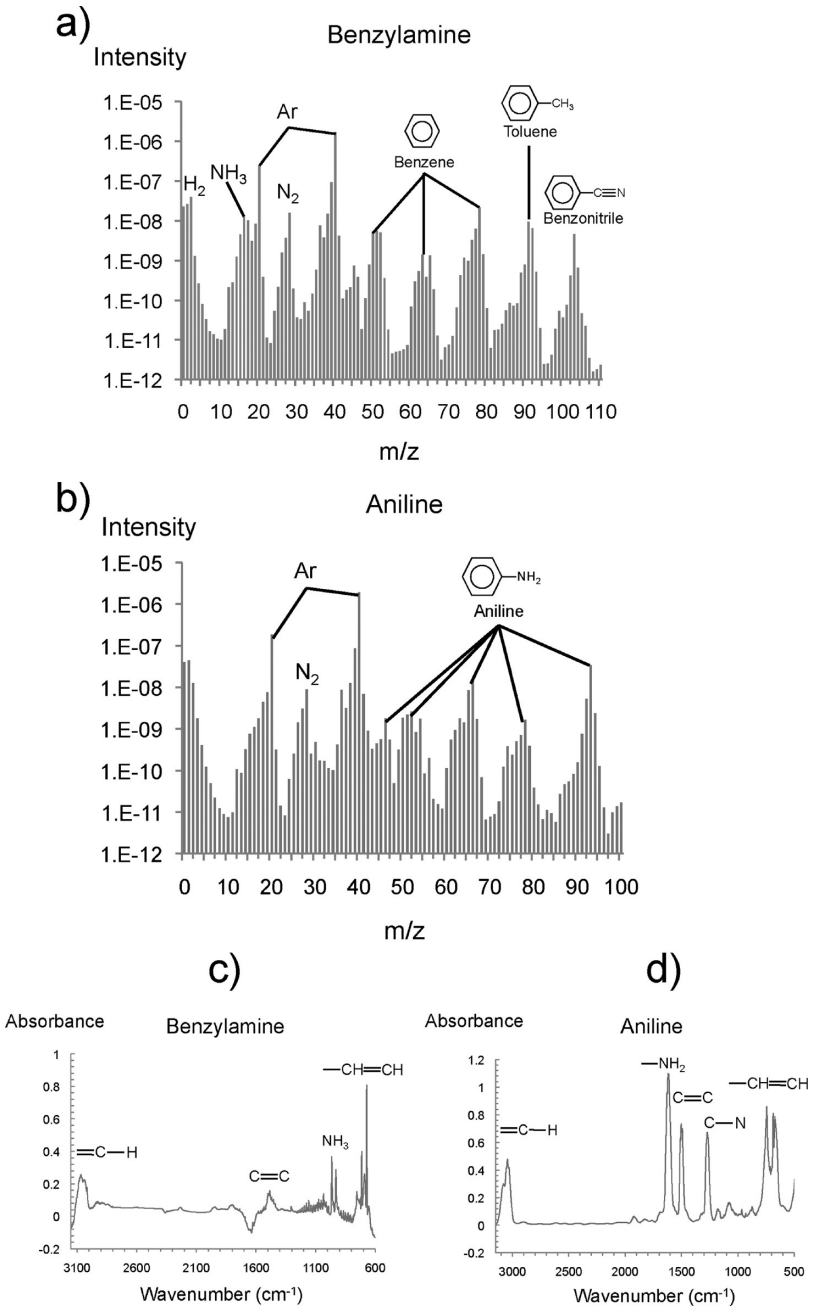

Figure 1. Mass spectra taken *in situ* under reaction conditions of (a) 5 wt % ferrocene and 95 wt % benzylamine, (b) 5 wt % ferrocene and 95 wt % aniline. FTIR spectra taken *in situ* under reaction conditions of (c) benzylamine and (d) aniline.

Ammonia in Carbon Nanotube Synthesis. To test whether ammonia can interact with the catalyst to produce single chiral angle CNTs, and to explore the role it plays in CNT chiral angle control, we directly passed ammonia into the reactor at different flow rates, alongside 5 wt % ferrocene in toluene. The flow rate of 3.0 mL/min corresponded to a molar concentration of approximately 1.4% in the feedstock solution, similar to that used previously with heteroatomic molecules. This concentration of ammonia produced the single chiral angle nanotubes seen in Figure 2. These featured the thick walls, internal membranes, and low N content (1.1 wt %) characteristic of this type of CNT.

The nanotubes produced at 30 mL/min of ammonia typically appear as in Figure 3, featuring multiple chiral angles and being noticeably disordered with relatively thin walls. The catalyst is also Fe_3C but more rounded as in Figure 3a. While the shape of the internal chambers reflects the shape of the catalyst particle, there appears to be no orientational relationship between the nanotube axis and the catalyst (Figure 3c). The nitrogen content of these CNTs, at 14 wt %, is also significantly higher than that of single chiral angle CNTs.

Catalyst Restructuring by Ammonia. From these observations and the literature, we can build an understanding of how ammonia causes the formation of catalyst

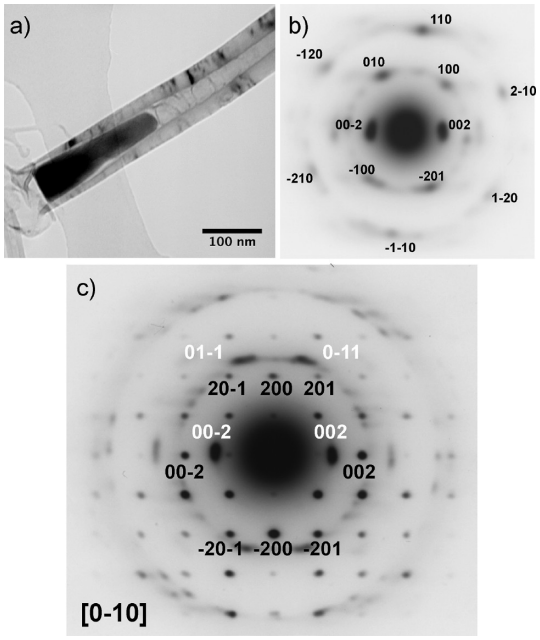

Figure 2. Images taken of CNT samples produced at 3 mL/min ammonia. (a) Bright-field TEM image of CNT and catalyst. Visible is the characteristic conical shape of the catalyst as well as the thick walls and internal membranes always found in single chiral angle CNTs. (b) Electron diffraction pattern from such a nanotube indicating that all of the layers have armchair chiral angle. (c) Electron diffraction pattern of CNT catalyst showing that it is Fe_3C and that the nanotube axis is parallel to the [100] plane of the catalyst, as is typical for single chiral angle CNTs. Catalyst reflections are labeled in black, CNT reflections in white.

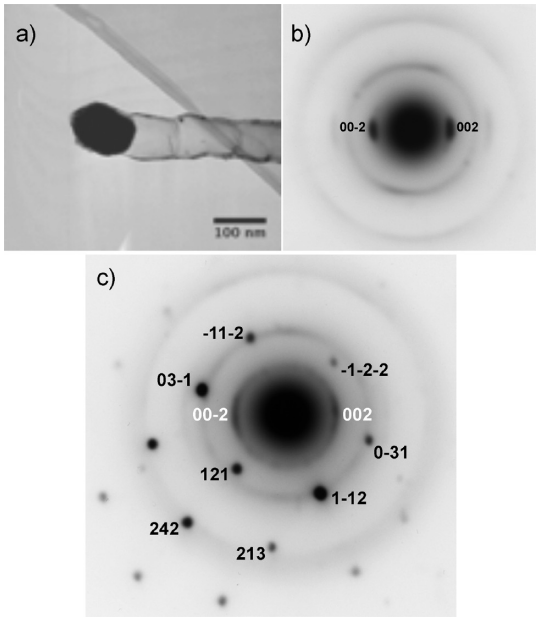

Figure 3. TEM images taken from samples produced at 30 mL/min ammonia. (a) Bright-field TEM image of the CNT and its catalyst particle. The walls are disordered and thin, though internal membranes are still present. The catalyst particle is also more uneven and rounded. (b) Electron diffraction pattern produced by CNT made at 30 mL/min; the continuous rings indicate that it contains layers with different chiral angles. The only distinct reflections are those of the 002 basal plane of the CNT. (c) Electron diffraction pattern produced by catalyst grown at 30 mL/min ammonia, which is consistent with an alignment near the [−513] zone axis of Fe_3C. Catalyst reflections are labeled in black, CNT reflections in white. There appears to be no orientational relationship between the CNT axis and the catalyst particle.

particles that are able to epitaxially grow CNTs and thereby control CNT chiral angle. Fe−N−C systems have been studied extensively in metallurgy, where ammonia has been shown to "open" the bcc Fe lattice, which has very low carbon solubility, to fcc Fe, which has a significantly higher carbon solubility.[27] It also stabilizes Fe_3C in steels.[28] These findings help us to explain our observation that CNT catalyst particles that produce single chiral angle CNTs are always Fe_3C: nitrogen transforms the bcc Fe to fcc Fe, thereby allowing the carbon concentration in the catalyst particle to increase and subsequently acting to stabilize Fe_3C. The formation of an Fe_3C catalyst particle is not enough, on its own, to control chiral angle, however, since multichiral angle CNTs have been shown to grow from Fe_3C in the literature[29] and in our work at 30 mL/min ammonia (Figure 3).

An important additional effect of ammonia is that it changes CNT nucleation kinetics. The addition of ammonia to a carburizing atmosphere has been shown to cause the formation of large Fe_3C deposits in bcc iron and thereby to suppress carbon precipitation.[30] The formation of Fe_3C has the concurrent effect of decreasing the carbon activity of the catalyst particle and thus also decreasing the driving force for the formation of carbon on the catalyst surface.[31] That the addition of pyrazine to synthesis at 660 °C in our reactor prevents the growth of CNTs is evidence that carbon activity is reduced by the addition of nitrogen. Ammonia therefore delays carbon precipitation and ensures that initial nanotube nucleation occurs from an active Fe_3C catalyst.

In the absence of ammonia, carbon will precipitate first, as has been experimentally observed in carburization of iron,[32] because the activity of carbon required for graphene precipitation is lower than that for Fe_3C.[33] The precipitation of a carbon layer before the formation of an active Fe_3C catalyst will increase the risk of catalyst deactivation. Ammonia therefore may increase the proportion of catalyst that is activated, accounting for the exceptionally high CNT densities observed in the single chiral angle CNT arrays (Table 1). This could also be an explanation for why ammonia is widely used to "activate" catalyst prior to CNT synthesis,[17−19] the reason for its effectiveness at this having hitherto been unclear.

CNT growth appears to cause substantial deformation of the catalyst;[34−38] therefore, the formation of an Fe_3C catalyst particle prior to graphene precipitation could contribute to the ability of the catalyst particle to assume a preferred orientation (Figure 2). This is further supported by Fe_3C appearing to occasionally form needle-like shapes in bcc Fe in a carburizing

atmosphere with ammonia.[30] Fe_3C has also been observed to feature preferential growth in the [100] direction when grown with a needle texture in a cast iron (n.b. the unit cell in this reference is labeled such that the growth direction is along the *b* axis).[39] The constant orientation of the catalyst particle with respect to the nanotube is likely to be a crucial factor in chiral angle control. This is supported by the observation that the orientation of the Fe_3C producing multichiral angle CNTs is constantly changing.[29]

The stabilization of Fe_3C, delay in carbon precipitation, and perhaps even the oriented growth of the catalyst particle prior to CNT nucleation should all occur at the higher ammonia concentration as well as the lower. The nanotubes grown at 30 mL/min ammonia, however, have multiple chiral angles, do not feature an orientational relationship with the catalyst from which they are grown (Figure 3), and have a more irregular appearance (similar to nanotubes more usually associated with ammonia in CNT synthesis[17]) than their counterparts producing single chiral angle CNTs (Figure 2). This difference suggests that ammonia has an additional, concentration-dependent, effect on the catalyst that is necessary for persistently controlling the orientation of the catalyst particle and also for chiral angle control.

At 3 mL/min ammonia, the CNT catalyst surface (Figure 4a) is reconstructed similarly to that in our previous report using pyrazine as the nitrogen source[23] and is suitable for epitaxial CNT growth. This reconstruction, specifically the structural change from iron carbide to iron, in the surface layer occurs because there is neither a stable nor a metastable equilibrium between Fe_3C and graphite.[40] Thus, following carbon supersaturation of the Fe_3C catalyst, carbon will precipitate and cause the Fe_3C to decompose, leaving the thin layer of iron between the carbide and the carbon that is observed. Such a layer has also been observed in decomposition of bulk Fe_3C, though it disappears at high carbon activity.[41] The epitaxial nucleation of graphene on this surface and its subsequent growth as a "belt" to form a nanotube then lead to both the chiral angle control[23] and, through the restraint imposed by the epitaxially matched nanotube, the persistence of the orientational relationship with the catalyst particle.

Such a process should also occur in the sample produced at 30 mL/min ammonia. However, the catalyst/nanotube interface produced at this ammonia flow rate (Figure 4b) does not suggest the epitaxial matching found in single chiral angle catalyst particles, and no pure iron layer is visible. We suggest that the higher nitrogen activity in the catalyst particle stabilizes Fe_3C to such an extent that it prevents iron surface layer formation. Without epitaxy at the interface, there is no means for chiral angle control, and the nanotube does not constrain the catalyst as it grows but rather distorts it, resulting in the absence of an orientational relationship between the two.

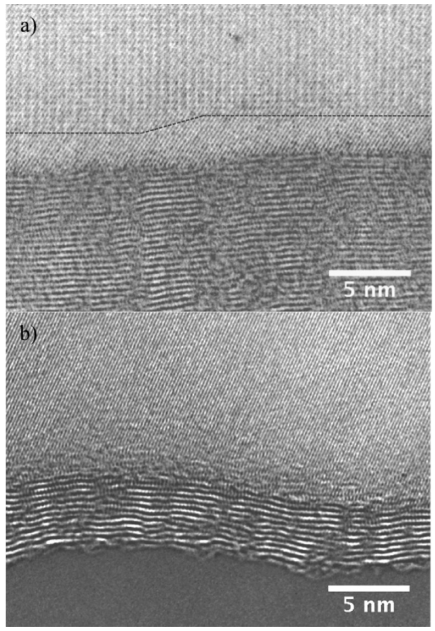

Figure 4. High-resolution TEM images of the catalyst/nanotube interface from a sample grown at (a) 3 mL/min ammonia and (b) 30 mL/min ammonia. In the lower ammonia concentration sample, the surface of the catalyst is reconstructed, as indicated by the dotted line, which is typical of a catalyst that produces single chiral angle nanotubes. In the higher ammonia concentration sample, there appears to be no restructuring of the catalyst surface to epitaxially grow the graphene, and the interfacial catalyst layer appears identical to its bulk.

In addition to the effects described above, it is worth mentioning that there is evidence that ammonia treatment can restructure iron catalyst surfaces, for instance, in ammonia synthesis.[42,43] Ammonia also appears to produce almost close-packed surfaces on iron single crystals.[44] Additionally, ammonia has been shown to induce extensive faceting on an iron wire near our reaction temperatures.[45] It is interesting to consider that ammonia may also act on any exposed pure iron surface of the catalyst to induce faceting or close packing and thereby aid the formation of a surface for epitaxial nanotube growth.

Future Strategies for the Use of Nitrogen in CNT Synthesis and Chiral Angle Control. Due to the range of different nitrogen sources that are able to produce single chiral angle CNTs, it is likely that ammonia is not the only nitrogen intermediate able to induce catalyst restructuring for epitaxial CNT growth. Indeed, ammonia completely decomposes on some iron surfaces at 127 °C and is thus very likely to be completely dissociated on contact with the catalyst.[46] Furthermore, the nitrogen sources investigated that produce multichiral angle CNTs either have low nitrogen availability, such as aniline and nitrogen gas, or high nitrogen availability, such as ammonia at 30 mL/min. We therefore suggest that the key requirement of the nitrogen source is that it has

sufficient chemical potential to cause catalyst reconstruction, but not so much that it prevents the formation of a reconstructed layer at the catalyst surface.

This model suggests that the primary components necessary for controlling the catalyst surface are the nitrogen and carbon activity in the catalyst. Variation of these could result in different surfaces and potentially also different chiral angles, and indeed, carbon source pressure has already been shown to change CNT chiral angle distributions.[47] The simple variation of nitrogen and carbon source concentrations in the reactor would be a very attractive and economical means of chiral angle control.

The addition of a small amount of nitrogen could easily be applied to increase CNT and graphene yield in many different synthesis processes. Similarly, epitaxial synthesis of graphene through nitrogen addition could significantly enhance product crystallinity. It is also encouraging that other transition metals appear to benefit from "activation" by ammonia,[17−19] suggesting that surface reconstruction might be induced in these, as well, again potentially leading to different chiral angle distributions.

It should also be emphasized that the surface from which the graphene epitaxially grows cannot be formed in pure fcc Fe crystals because the hexagonally structured planes in these are tetrahedrally disposed with respect to each other and therefore not compatible with the uniaxial symmetry of the nanotube. The underlying Fe_3C layer provides a symmetry base that allows a hexagonally structured surface that is compatible with the nanotube symmetry to form. Novel surface geometries such as this that rely on the presence of multiple catalyst phases could be useful in processes in which iron is already used as a catalyst, such as ammonia synthesis, or applied to other areas of catalysis.

CONCLUSION

We have investigated the different nitrogen-containing additives that result in the growth of single chiral angle CNTs from ordered catalyst particles. Our *in situ* study of the synthesis of single chiral angle CNTs suggested that nitrogen interacted with the catalyst in the form of ammonia. We confirmed that ammonia is a suitable nitrogen source for the production of single chiral angle CNTs by epitaxial growth from a reconstructed surface, similar to those produced using other nitrogen sources. In excess ammonia, however, this reconstructed layer is absent, resulting in multichiral angle CNTs. We surmise that any nitrogen source with appropriate chemical potential is able to produce highly ordered catalyst particles that epitaxially grow CNTs, and that the mechanism for this relies on an appropriate level of carbon activity in, and carbide stabilization of, the catalyst. This mechanism also offers an explanation for why ammonia is widely used to activate catalyst prior to CNT growth. These findings suggest a simple and economical new strategy for CNT chiral angle control, improving CNT and graphene yield and crystallinity, and highlight the uses of novel surface geometries achievable through multiphase catalysts.

METHODS

Our system was based on the thermal CVD setup with vapor phase catalyst injection used by Singh *et al.*[48] The feedstock was prepared by mixing the nitrogen source with toluene and 5 wt % ferrocene and then ultrasonicated for 10 min. A Hamilton Gastight syringe was used to inject the feedstock at 5.6 mL/h into a stainless steel tube, heated to 180 °C to evaporate the feedstock, leading into the sealed quartz tube in the hot zone of the furnace where the synthesis took place. Argon was used as carrier gas at 1 L/min to carry the feedstock into the furnace hot zone at 760 °C. The mass spectrometer (Omnistar) with a channeltron detector used a quartz capillary tube that was inserted directly into the hot zone of the furnace *via* a side arm in the quartz reaction vessel. The FTIR quartz sample tube was inserted similarly using the side arm. Scanning electron microscopy (SEM) was carried out using a JEOL 6340F microscope. Transmission electron microscopy (TEM) was done using JEOL 4000EX and JEOL 200CX. Nitrogen content in the CNTs was measured by combustion analysis.

Conflict of Interest: The authors declare no competing financial interest.

Acknowledgment. The authors thank C. Ducati for stimulating discussions. S.P. would like to thank the EPSRC for funding. K.K. would like to thank the Royal Society and the ERC for funding.

REFERENCES AND NOTES

1. Arnold, M. S.; Green, A. A.; Hulvat, J. F.; Stupp, S. I.; Hersam, M. C. Sorting Carbon Nanotubes by Electronic Structure Using Density Differentiation. *Nat. Nanotechnol.* **2006**, *1*, 60–65.
2. Zheng, M.; Jagota, A.; Strano, M. S.; Santos, A. P.; Barone, P.; Chou, S. G.; Diner, B. A.; Dresselhaus, M. S.; McLean, R. S.; Onoa, G. B.; *et al.* Structure-Based Carbon Nanotube Sorting by Sequence-Dependent DNA Assembly. *Science* **2003**, *302*, 1545–1548.
3. Zhang, G. Y.; Qi, P. F.; Wang, X. R.; Lu, Y. R.; Li, X. L.; Tu, R.; Bangsaruntip, S.; Mann, D.; Zhang, L.; Dai, H. J. Selective Etching of Metallic Carbon Nanotubes by Gas-Phase Reaction. *Science* **2006**, *314*, 974–977.
4. Voggu, R.; Rao, K. V.; George, S. J.; Rao, C. N. R. A Simple Method of Separating Metallic and Semiconducting Single-Walled Carbon Nanotubes Based on Molecular Charge Transfer. *J. Am. Chem. Soc.* **2010**, *132*, 5560–5561.
5. Tanaka, T.; Jin, H.; Miyata, Y.; Fujii, S.; Suga, H.; Naitoh, Y; Minari, T.; Miyadera, T.; Tsukagoshi, K.; Kataura, H. Simple and Scalable Gel-Based Separation of Metallic and Semiconducting Carbon Nanotubes. *Nano Lett.* **2009**, *9*, 1497–1500.
6. Yu, B.; Hou, P. X.; Li, F.; Liu, B. L.; Liu, C.; Cheng, H. M. Selective Removal of Metallic Single-Walled Carbon Nanotubes by Combined *In Situ* and Post-Synthesis Oxidation. *Carbon* **2010**, *48*, 2941–2947.
7. Tu, X.; Manohar, S.; Jagota, A.; Zheng, M. DNA Sequence Motifs for Structure-Specific Recognition and Separation of Carbon Nanotubes. *Nature* **2009**, *460*, 250–253.
8. Harutyunyan, R. A.; Chen, G.; Paronyan, T. M.; Pigos, E. M.; Kuznetsox, O. A.; Hewaparakrama, K.; Kim, S. M.; Zakharov, D.; Stach, E. A.; Sumanasekera, G. U. Preferential Growth of Single-Walled Carbon Nanotubes with Metallic Conductivity. *Science* **2009**, *326*, 116–120.
9. Hong, G.; Zhang, B.; Peng, B.; Zhang, J.; Choi, W.; Choi, J.; Kim, J.; Liu, Z. Direct Growth of Semiconducting

Single-Walled Carbon Nanotube Array. *J. Am. Chem. Soc.* **2009**, *131*, 14642–14643.
10. Ding, L.; Tselev, A.; Wang, J. Y.; Yuan, D. N.; Chu, H. B.; McNicholas, T. P.; Li, Y.; Liu, J. Selective Growth of Well-Aligned Semiconducting Single-Walled Carbon Nanotubes. *Nano Lett.* **2009**, *9*, 800–805.
11. Loebick, C. Z.; Podila, R.; Reppert, J.; Chudow, J.; Ren, F.; Haller, G. L.; Rao, A. M.; Pfefferle, L. D. Selective Synthesis of Subnanometer Diameter Semiconducting Single-Walled Carbon Nanotubes. *J. Am. Chem. Soc.* **2010**, *132*, 11125–11131.
12. Ghorannevis, Z.; Kato, T.; Kaneko, T.; Hatakeyama., R. Narrow-Chirality Distributed Single-Walled Carbon Nanotube Growth from Nonmagnetic Catalyst. *J. Am. Chem. Soc.* **2010**, *132*, 9570–9572.
13. Qu, L. T.; Du, F.; Dai, L. M. Preferential Syntheses of Semiconducting Vertically Aligned Single-Walled Carbon Nanotubes for Direct Use in FETs. *Nano Lett.* **2008**, *8*, 2682–2687.
14. Xu, Z.; Bai, X.; Wang, Z. L.; Wang, E. Multiwall Carbon Nanotubes Made of Monochirality Graphite Shells. *J. Am. Chem. Soc.* **2006**, *128*, 1052–1053.
15. Ruland, W.; Schaper, A. K.; Hou, H.; Greiner, A. Multi-Wall Carbon Nanotubes with Uniform Chirality: Evidence for Scroll Structures. *Carbon* **2003**, *41*, 423–427.
16. Ducati, C.; Koziol, K.; Friedrichs, S.; Yates, T.; Shaffer, M.; Midgley, P.; Windle, A. H. Crystallographic Order in Multi-Walled Carbon Nanotubes Synthesized in the Presence of Nitrogen. *Small* **2006**, *2*, 774–784.
17. Ducati, C.; Alexandrou, I.; Chhowalla, M.; Amaratunga, G.; Robertson, J. Temperature Selective Growth of Carbon Nanotubes by Chemical Vapor Deposition. *J. Appl. Phys.* **2002**, *92*, 3299–3303.
18. Hofmann, S.; Cantoro, M.; Kleinsorge, B.; Casiraghi, C.; Parvez, A.; Robertson, J.; Ducati, C. Effects of Catalyst Film Thickness on Plasma-Enhanced Carbon Nanotube Growth. *J. Appl. Phys.* **2005**, *98*, 034308.
19. Jang, Y. T.; Ahn, J.-H.; Lee, Y.-H.; Ju, B.-K. Effect of NH_3 and Thickness of Catalyst on Growth of Carbon Nanotubes Using Thermal Chemical Vapor Deposition. *Chem. Phys. Lett.* **2003**, *372*, 745–749.
20. Hofmann, S.; Sharma, R.; Ducati., C.; Du, G.; Mattevi, C.; Cepek, C.; Cantoro, M.; Pisana, S.; Parvez, A.; Cervantes-Sodi, F.; *et al. In Situ* Observations of Catalyst Dynamics during Surface-Bound Carbon Nanotube Nucleation. *Nano Lett.* **2007**, *7*, 602–608.
21. Zhu, Z.; Jiang, H.; Susi, T.; Nasibulin, A. G; Kauppinen, E. I. The Use of NH_3 To Promote the Production of Large-Diameter Single-Walled Carbon Nanotubes with a Narrow (*n*,*m*) Distribution. *J. Am. Chem. Soc.* **2011**, *133*, 1224–1227.
22. Koziol, K. K. K.; Shaffer, M.; Windle, A. H. Three-Dimensional Internal Order in Multiwalled Carbon Nanotubes Grown by Chemical Vapor Deposition. *Adv. Mater.* **2005**, *17*, 760–763.
23. Koziol, K. K. K.; Ducati, C.; Windle, A. H. Carbon Nanotubes with Catalyst Controlled Chiral Angle. *Chem. Mater.* **2010**, *22*, 4904–4911.
24. Pattinson, S. W.; Prehn, K.; Kinloch, I. A.; Eder, D; Koziol, K. K. K.; Schulte, K.; Windle, A. H. The Life and Death of Carbon Nanotubes. *RSC Adv.* **2012**, *2*, 2909–2913.
25. Song, S.; Golden, D. M.; Hanson, R. K.; Bowman, C. T. A Shock Tube Study of Benzylamine Decomposition: Overall Rate Coefficient and Heat of Formation of the Benzyl Radical. *J. Phys. Chem. A* **2002**, *106*, 6094–6098.
26. Rylander, P. N.; Meyerson, S.; Eliel, E. L.; McCollum, J. D. Organic Ions in the Gas Phase. XII. Aniline. *J. Am. Chem. Soc.* **1963**, *85*, 2723–2725.
27. Jack, K. H. Binary and Ternary Interstitial Alloys. II. The Iron-Carbon-Nitrogen System. *Proc. R. Soc. London, Ser. A* **1948**, *1040*, 41–55.
28. Kagawa, A.; Okamoto, T. Partition of Nitrogen in Hypo-Eutectic and nearly Eutectic Iron-Carbon Alloys. *Mater. Trans.* **1981**, *22*, 137–143.
29. Yoshida, H.; Takeda, S.; Uchiyama, T.; Kohno, H.; Homma, Y. Atomic-Scale *In-Situ* Observation of Carbon Nanotube Growth from Solid State Iron Carbide Nanoparticles. *Nano Lett.* **2008**, *8*, 2082–2086.
30. Gressmann, T.; Nikolussi, M; Leineweber, A.; Mittemeijer, E. J. Formation of Massive Cementite Layers on Iron by Ferritic Carburising in the Additional Presence of Ammonia. *Scripta Mater.* **2006**, *55*, 723–726.
31. Hillert, M.; Selleby, M. Discussion of Cementite Layer Formation and Sooting. *Scripta Mater.* **2010**, *63*, 1037–1040.
32. Zhang, J.; Schneider, A.; Inden, G. Initiation and Growth of Iron Metal Dusting in $CO-H_2-H_2O$ Gas Mixtures. *Corros. Sci.* **2007**, *50*, 1020–1034.
33. Szakalos, P. Mechanisms and Driving Forces of Metal Dusting. *Mater. Corros.* **2003**, *54*, 752–762.
34. Zhu, H.; Suenaga, K.; Hashimoto, A.; Urita, K.; Hata, K.; Ijima, S. Atomic-Resolution Imaging of the Nucleation Points of Single-Walled Carbon Nanotubes. *Small* **2005**, *1*, 1180–1183.
35. Begtrup, G. E.; Gannett, W.; Meyer, J. C.; Yuzvinsky, T. D.; Ertekin, E.; Grossman, J. C.; Zettl, A. Facets of Nanotube Synthesis: High-Resolution Transmission Electron Microscopy Study and Density Functional Theory Calculations. *Phys. Rev. B* **2009**, *79*, 205409.
36. Moors, M.; Amara, H.; de Bocarme, T. V.; Bichara, C.; Ducastelle, F.; Kruse, N.; Charlier, J.-C. Early Stages in the Nucleation Process of Carbon Nanotubes. *ACS Nano* **2009**, *3*, 511–516.
37. Pigos, E.; Penev, E. S.; Ribas, M. A.; Sharma, R.; Yakobson, B. I.; Harutyunyan, A. R. Carbon Nanotube Nucleation Driven by Catalyst Morphology Dynamics. *ACS Nano* **2011**, *5*, 10096–10101.
38. Behr, M. J.; Mkhoyan, K. A.; Aydil, E. S. Catalyst Rotation, Twisting, and Bending during Multiwall Carbon Nanotube Growth. *Carbon* **2010**, *48*, 3840–3845.
39. Hartmann, S.; Ruppersberg, H. Thermal Expansion of Cementite and Thermoelastic Stresses in White Cast Iron. *Mater. Sci. Eng., A* **1995**, *190*, 231–239.
40. Kim, H.; Sigmund, W. Iron Particles in Carbon Nanotubes. *Carbon* **2005**, *43*, 1743–1748.
41. Zhang, J.; Schneider, A.; Inden, G. α-Fe Layer Formation during Metal Dusting of Iron in $CO-H_2-H_2O$ Gas Mixtures. *Mater. Corros.* **2003**, *54*, 763–769.
42. Strongin, D. R.; Somorjai, G. A. Ammonia-Pretreatment-Induced Restructuring of Iron Single-Crystal Surfaces: Its Effects on Ammonia Synthesis and on Coadsorbed Aluminum Oxide and Potassium. *J. Catal.* **1989**, *118*, 99–110.
43. Dumesic, J. A.; Topsoe, H.; Boudart, M. Surface, Catalytic and Magnetic Properties of Small Iron Particles: III. Nitrogen Induced Surface Reconstruction. *J. Catal.* **1975**, *37*, 513–522.
44. Escott, D. K.; Pratt, S. J.; King., D. A. Evidence for a Nitrogen-Induced Reconstruction of Fe{111}. *Surf. Sci.* **2004**, *562*, 226–236.
45. Loffler, D. G.; Schmidt, L. D. Kinetics of NH_3 Decomposition on Iron at High Temperatures. *J. Catal.* **1976**, *44*, 244–258.
46. Weiss, M.; Ertl, G.; Nitschke, F. Adsorption and Decomposition of Ammonia on Fe(110). *Appl. Surf. Sci.* **1979**, *2*, 614–635.
47. Wang, B.; Wei, L.; Yao, L.; Li, L.-J.; Yang, Y.; Chen, Y. Pressure-Induced Single-Walled Carbon Nanotube (*n*,*m*) Selectivity on Co–Mo Catalysts. *J. Phys. Chem. C* **2007**, *111*, 14612–14616.
48. Singh, C.; Shaffer, M. S. P.; Windle, A. H. Production of Controlled Architectures of Aligned Carbon Nanotubes by an Injection Chemical Vapour Deposition Method. *Carbon* **2003**, *41*, 359–368.